See discussions, stats, and author profiles for this publication at: https://www.researchgate.net/publication/296461905

Design Considerations of a Lift-Offset Single Main Rotor Compound Helicopter

Conference Paper · January 2016

CITATIONS
15

READS
6,043

4 authors, including:

Ananth Sridharan

33 PUBLICATIONS **224** CITATIONS

SEE PROFILE

Bharath Govindarajan
University of Maryland, College Park

33 PUBLICATIONS **515** CITATIONS

SEE PROFILE

Inderjit Chopra
University of Maryland, College Park

532 PUBLICATIONS **13,086** CITATIONS

SEE PROFILE

All content following this page was uploaded by Ananth Sridharan on 01 March 2016.

The user has requested enhancement of the downloaded file.

Design Considerations of a Lift-Offset Single Main Rotor Compound Helicopter

Ananth Sridharan [*] Bharath Govindarajan [†] V. T. Nagaraj [‡] Inderjit Chopra [§]
Department of Aerospace Engineering, University of Maryland, College Park, MD

ABSTRACT

This paper investigates design trends and performance trade-offs for a lift- and thrust-augmented asymmetric single main rotor helicopter. The primary goal of introducing lift and thrust augmentation is to increase the cruise speed to upward of 200 knots for the same payload and range of a conventional medium-lift utility helicopter. The configuration of interest is also compared to a thrust-augmented coaxial design. The convergence process was initiated using multi-parameter sweeps with a simple performance model that filters out unrealistic combinations of design parameters based on blade loading and rotor lift offset. After applying this initial filter, additional design iterations were carried out using comprehensive analysis directly to calculate rotor power on-line for sizing. The second step, while relatively slow, still executes within minutes, and incorporates physics-based rotor performance models without apriori tuning of power factors or coefficients. Using the methodology, a thrust and lift-augmented asymmetric compound helicopter was designed with blade-level optimization. This configuration has a lower installed power and fuel requirements compared to a thrust-augmented coaxial helicopter, for the mission chosen herein.

NOMENCLATURE

a	Speed of sound, ft/s
A	Rotor disk area, ft^2
AR_{wing}	Fixed wing aspect ratio
C_{d_0}	Profile drag coefficient of rotor airfoil sections
$C_{D_{0W}}$	Mean profile drag coefficient of fixed wing
C_{L_W}	Operating lift coefficient of fixed wing
C_T	Rotor Thrust Coefficient, $= T/(\rho A(\Omega R)^2)$
e	Ostwald efficiency factor for fixed wing
f	Fuselage equivalent flat-plate area, ft^2
K_f	Flat plate trend proportionality constant, ft^2
M	Local Mach number
$M_{tip,cr}$	Advancing tip Mach number limit in cruise
N_b	Number of blades per rotor
N_R	Number of rotors
P_{cr}	Shaft power required in cruise, hp
$P_{i,H}$	Induced power in hover for all rotors, hp
$P_{o,H}$	Profile power in hover for all rotors, hp
P_H	Shaft power required to hover, hp
P_{prop}	Propeller power, hp
R	Rotor radius, ft
S_{wing}	Fixed wing plan-form area, ft^2
T	Thrust per rotor, lb
T_{prop}	Propeller thrust, lb
v_i	Induced inflow velocity, ft/s
V_∞	Flight speed, ft/s
W	Gross Take-off Weight, lb
W_{cr}	Weight during Cruise Segment, lb
α_{TPP}	Forward tip-path-plane tilt, radians
η_p	Propeller efficiency ratio
κ_C	Induced power factor in cruise
κ_H	Induced power factor in hover
κ_{int}	Coaxial interference factor for induced power
λ_i	Induced inflow ratio, $= v_i/(\Omega R)$
λ	Inflow ratio
ρ	Air density, slug/ft^3
σ	Rotor solidity
Ω	Rotor rotational speed, rad/s
μ	Advance ratio, $= V_\infty/(\Omega R)$

LIST OF ABBREVIATIONS

ROM	Reduced Order Model
CSD	Computational Structural Dynamics

INTRODUCTION

The conventional single main rotor helicopter was conceptualized as a means to achieve vertical lift, with some limited ability to fly forwards. At high forward flight speeds, the onset of compressibility on the advancing blade tips and airfoil dynamic stall on the retreating side introduce vibratory loads that rapidly consume allowable fatigue cycles in the structure. The imbalance in dynamic pressure between the advancing and retreating sides of the rotor disk renders rolling moment balance an impossible goal at high advance ratios.

---

[*] Research Associate, E-mail: ananth@umd.edu
[†] Research Associate, E-mail: bharath@umd.edu
[‡] Senior Research Scientist, E-mail: vnagaraj@umd.edu
[§] Professor, E-mail: chopra@umd.edu

Presented at the American Helicopter Society technical meeting on Aeromechanics Design for Vertical Lift, San Francisco, CA, January 20–22, 2016.

Thus, various aspects of rotor aerodynamics and aeromechanics limit the maximum forward flight speed to approximately 160 knots for a single-rotor helicopter, which falls well short of the 200+ knots required for next-generation high-speed rotorcraft. The coaxial compound and the tilt-rotor are two popular designs suited to high-speed forward flight. While the aerodynamic efficiency of a prop-rotor easily exceeds that of a rotor flying edgewise, maintenance and operating costs associated with the tilt-rotor are significant. In a coaxial rotor system, the presence of two swashplates introduces a combination of control system complexity, excessive mast drag and/or hub weight penalties because of high blade flap stiffness, primarily driven by allowable inter-rotor tip clearances. Instead of the coaxial or tilt-rotor configurations, this paper investigates a third option for a platform with simultaneous VTOL capabilities and high-speed cruise: the so-called lift-offset single main rotor with lift and thrust compounding.

The configuration being proposed is an evolution of a conventional single main rotor/tail rotor helicopter. Lift and thrust augmentation devices are functionally near-identical to the coaxial compound system. The key feature is that instead of using another *rotor* to balance the hub rolling moment, this configuration uses an *asymmetric fixed wing* as shown in Fig. 1. The advantages of this configuration are :

1. **Slowed main rotor**: at high forward flight speeds, compressibility drag on the advancing blade tips is a major concern for both performance and hub vibrations. By reducing or eliminating the source of the loading, the associated penalties are avoided.

2. **Asymmetric fixed wing**: at high forward flight speeds, the fixed wing on the retreating side simultaneously alleviates rotor thrust requirements *and* provides a counter moment to allow for trimmed forward flight. A movable trailing edge flap is used to regulate the lift and allows for smooth variation over a range of flight speeds.

3. **Swiveling tail rotor**: At 100 knots, the anti-torque function is transferred to the vertical fin and the tail rotor is off-loaded, powered down and swiveled to propeller mode. After swiveling is complete, the propeller is powered by the engine and used to provide propulsive thrust. The main rotor can be used to generate vertical thrust alone in high-speed flight, avoiding excessive parasitic power penalties associated with fuselage drag at high angles of attack.

The prime disadvantage of this configuration is that the transmission deck and airframe need to be stronger than for a conventional helicopter, since the rolling moment from the wing and rotor hub need to be carried through the structure before canceling each other. A minor disadvantage is the download penalty in hover due to additional blockage created by the fixed wing.

The field of helicopter/rotorcraft conceptual design is driven by analysis, synthesis, and optimization to find the best configuration to perform a given mission and meet the required performance specifications. The process of design is often sequential with each step being increasingly complex in terms of the fidelity of the models used within these tools. However, increasing the fidelity comes with a penalty of computational cost, which make it impractical at the early design stages to use ”high-cost models” where numerous permutations of vehicle configurations have to be assessed to narrow down the potential design space. Therefore, design tools have historically been of low fidelity to facilitate rapid application to a wide number of design parameters (e.g., rotor disk loading, rotor tip speed, etc.). As configurations become more complex, such as the addition of a wing and/or propeller(s), there is a need to scan a larger design space as there is now an increase in the number of design parameters, which ultimately reflect on the total cost of computation. Furthermore, there is also a need to develop an accurate physics-based design tool

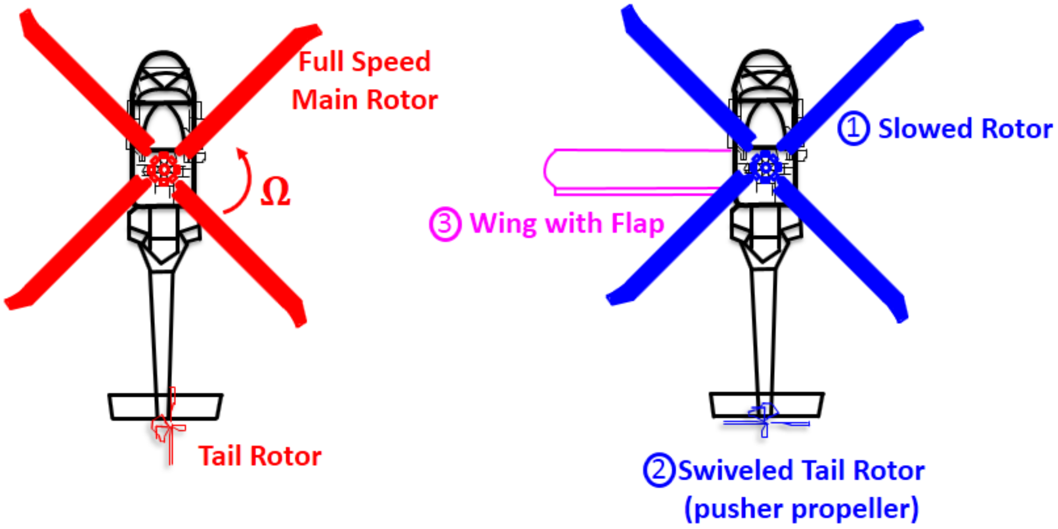

Fig. 1. Schematic representation of a baseline conventional helicopter (left) and a compound rotorcraft (right).

that is capable of capturing the physical phenomenon of some exotic concepts being designed.

Various design codes exist in literature and have been widely used by helicopter industries and universities, including NDARC (NASA), RDM (Sikorsky), PRESTO (Bell Helicopter) and HESCOMP and VASCOMP (Boeing). These tools contain simple physics based models with empirical corrections to evaluate the various aspects of vehicle performance and to evaluate the component weights. As configurations and concepts become increasingly complex, there is a need to introduce higher-fidelity models such as comprehensive analysis tools. Some examples of these tools include CAMRAD (NASA), RCAS (U.S. Army), DYMORE (Georgia Institute of Technology) and UMARC (University of Maryland); see Johnson (Ref. 1) for a detailed summary. These codes over various studies have been used to analyze concepts such as slowed-rotor compounds (Ref. 2), tilting-tandem concept (Ref. 3), compound gyroplanes (Ref. 4) and rotors with individual blade control (Ref. 5).

While a fair amount of literature exists on using design tools towards advanced rotorcraft configurations, there is a dearth in studies conducted towards the specific configuration of interest, i.e., a half-wing coupled with a lift-offset single rotor. A design with this configuration does exist for small-scale unmanned air vehicle (UAV) operations under the name “Challis Heliplane” (Ref. 6). However, references to the Heliplane in the literature are few, and detailed aeromechanics analyses are unavailable to the public-domain. A passing mention exists in a survey of small-scale UAVs by Cai et. al (Ref. 7). Design optimization results for reducing vehicle weight for various configurations, including the Challis Heliplane, are presented in the work by Vu et al. (Ref. 4). This work used a sizing analysis code and reduced-order models with analytical expressions to evaluate performance. While their design tool also contained an optimizer, the primary goal of the work was to validate the codes used against existing configurations. There was no improvements in design suggested for the configuration of interest. Sartorius (Ref. 8) and Cumbrebras and Sartorius (Ref. 9) studied a single rotor with lift-offset and a half wing for a 5,000 kg vehicle in high speed forward flight. They were able to show that the flight envelope could be extended to over 250 knots when compared to a maximum flight speed of 150 knots for the conventional single rotor configuration. Their study, however lacked a detailed study of the various design parameters and a study of the different sub-components of the vehicle at different flight conditions.

The primary objectives of the paper are two-fold: 1. To develop a conceptual design framework with the ability to include either simple performance equations or to directly import comprehensive analysis into the design iterations, and 2. To demonstrate the feasibility of the framework for a 20,000 lb (medium lift) GTOW for a single lift-offset rotor with a wing and propeller. Studies are conducted to vary the different design parameters and to study the performance of the vehicle at different flight conditions.

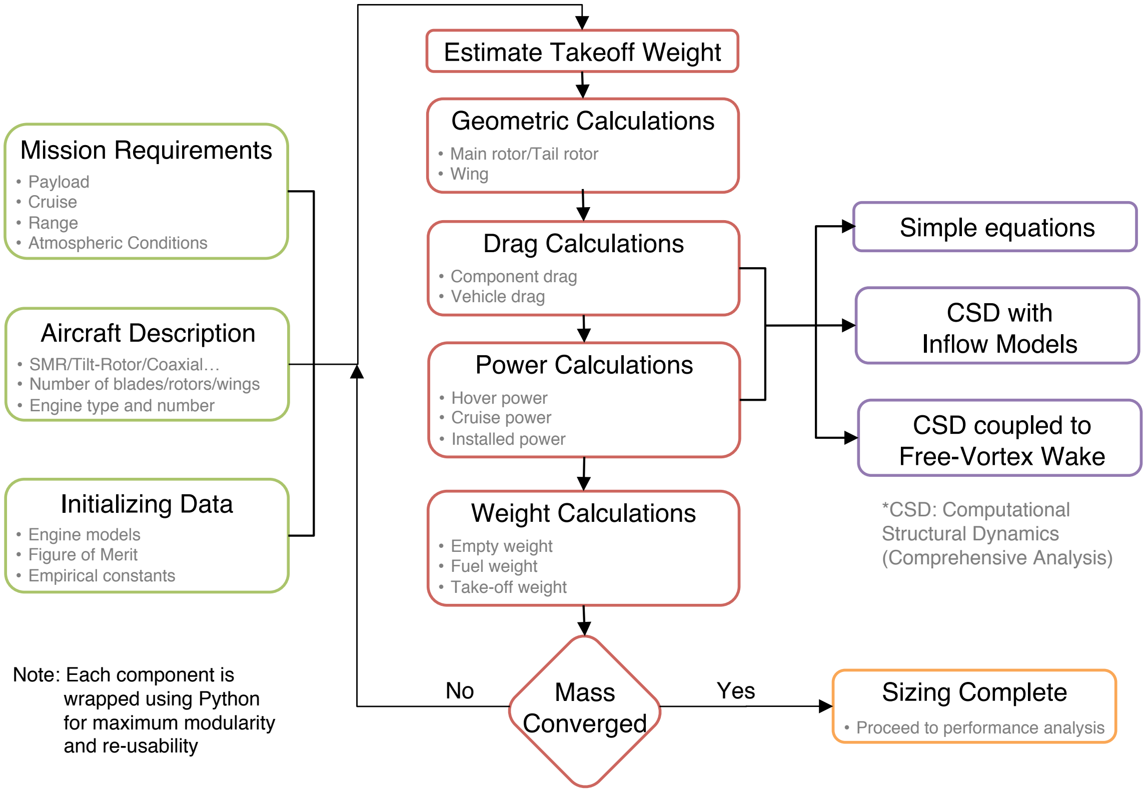

Fig. 2. Flowchart depicting the HYDRA framework.

METHODOLOGY

The developed HYbrid Design and Rotorcraft Analysis (HYDRA) tool is an integrated code suite that can perform conceptual rotorcraft design tasks for arbitrary user-selected rotorcraft configurations. These configurations include a conventional helicopter, coaxial compound with lift and thrust augmentation, tilt-rotor and asymmetric single rotor compounds. Although initially implemented with low-fidelity performance models typical of conceptual design environments, the architecture allows for multidisciplinary design, analysis and optimization. The framework was extended to encapsulate a comprehensive analysis code in the sizing process for accurate performance predictions, especially at high advance ratios. A flowchart depicting the interdependencies of the subcomponents of HYDRA are shown in Fig. 2. User input parameters and their respective ranges of values investigated in the present work are given in Table 1. Each component of HYDRA is described in the following section.

Rotor parameter	Range	Units
Disk Loading DL	6 – 20	lb/sq.ft
Rotor Solidity σ	0.05 – 0.15	
Number of blades N_b	3 – 6	
Hover tip speed V_{TIP}	195 – 240	m/s
Cruise tip Mach limit	0.8 – 0.9	
Wing parameter	**Range**	**Units**
Aspect ratio AR	4 – 10	
Lift fraction f_W	0 – 0.5	

Table 1. Design Parameters

Helicopter Sizing

The proposed vehicle is a hybrid between a fixed-wing aircraft and a conventional helicopter. A modified sizing method based on Tishchenko's original helicopter methodology (Ref. 10) is used to size the vehicle and provide estimates of the vehicle weights and power requirements. The description of the aircraft involves defining the number of engines and lifting/thrusting components (rotors, wings and propellers), and their relative placement and orientation. A representative mission profile consists of a idle, hover and cruise phases and the corresponding atmospheric conditions (i.e., density altitude and temperature) are used to estimate the maximum gross take-off weight, installed power and fuel required for a given payload mass. The sizing methodology has been validated against the NASA Design and Analysis of Rotorcraft (NDARC) code for various mission profiles (Ref. 11).

A schematic of the sizing algorithm is shown in Fig. 2. To ensure that the components contributing to aircraft empty weight are accurately represented, the weights equations presented in the NDARC (Ref. 12) report are used in HYDRAs sizing tool. The equations also account for wing-related components that are sized based on structural stiffness and loading requirements. Powerplant characteristics (engine weight and specific fuel consumption) are obtained based on nominal trends for turboshaft engines. The code was expanded to allow for power calculations using the comprehensive analysis during the design iterations. This inclusion of a higher-order models is critical for accurate performance predictions at advance ratios of 0.5 and above, where reliable test/empiricism-based tuning factors for low-fidelity models are not yet available. For high-speed configurations in which the main rotor operates with significant lift asymmetry between the advancing and retreating sides, a higher-fidelity flowfield model (free wake) that is more representative of the rotor flowfield is used in the present study. This process is similar to the approach used by Moodie and Yeo (Ref. 13), with one key improvement; rather than calibrate an approximate model with a higher-fidelity analysis tool, the approximate model is *replaced entirely* by the comprehensive analysis.

Empty Weight

Models developed by the U.S. Army Aeroflightdynamics Directorate (AFDD) (Ref. 12) were used to evaluate the contribution of different vehicle components to the empty weight. These weights are compiled from existing helicopters and tiltrotors, from which parametric equations were extracted; these calibrated trends were then used to predict the respective component weights. The horizontal and vertical tail areas are scaled linearly with rotor radius, calibrated to the UH60A. Engine weight is scaled linearly with the power required using the UH60A as a reference, i.e.

$$\text{Engine Weight} = \frac{450 \text{ lb}}{1620 \text{ Shp}} \times \text{Installed Power, hp.}$$

A list of the different weight groups along with their dominant dependencies are listed in Table 2. These dominant dependencies are the parameters that the empty weight of a given group is most sensitive to. The AFDD weight models allows for "technology factors" which, in effect reduce the empty weight by a chosen factor in anticipation of the advancement of technology over the years. However, in the present study, all technology factors were all set to one, i.e., no assumption was made for a decrease in weight based on future technologies. Therefore, the empty weight obtained through this procedure is a conservative estimate, in that is representative of current manufacturing proficiencies.

Power Calculations: Simplified Model

During design iterations, two models of different fidelity levels are available for estimation of rotor shaft torque and engine power requirements. The reduced-order model, implemented using momentum theory and an energy approach, does not explicitly model local effects such as varying blade geometry,

Group Name	Description	Dominant Dependencies
Fixed wing	AFDD93	Weight, wing aspect ratio
Rotor	AFDD00	Radius, solidity, flap frequency
Empennage	Custom	Radius
Propeller	AFDD82	Vehicle drag
Fuselage	AFDD82	Weight, radius
Alighting gear	AFDD82	Weight
Engine	Custom	Maximum power
Air induction	AFDD82	Engine weight
Fuel system	AFDD82	Fuel flow rate
Drive system	AFDD00	Maximum torque, rotor weight
Flight control and hydraulics	AFDD82	Rotor geometry
Deicing	AFDD	Rotor geometry

Table 2. Constituent Components of Empty Weight

tip compressibility or stall. Instead, these losses are folded into power factors that multiply the induced and profile power coefficients.

Hover: The breakdown of hover power is given by

$$
\begin{aligned}
P_{i_\mathrm{H}} &= N_\mathrm{R}\,\kappa_\mathrm{H}\frac{T^{3/2}}{\sqrt{2\rho A}} \\
P_{o_\mathrm{H}} &= N_\mathrm{R}\frac{\sigma C_{d_0}}{8}\rho A(\Omega R)^3 \\
P_\mathrm{H} &= \kappa_\mathrm{int} P_{i_\mathrm{H}} + P_{o_\mathrm{H}} \qquad (1)
\end{aligned}
$$

where N_R is the number of rotors, ρ is the local atmospheric density, A is the rotor disk area, C_{d_0} is mean profile drag coefficient and ΩR is the hover tip speed. $P_{i,H}$, $P_{o,H}$ and P_H are the induced, profile and total power in hover, respectively. The inter-rotor interference factor κ_int is set to 1.0 for single rotor designs, and 1.15 for coaxial rotors.

Cruise: In forward flight (i.e., cruise), the power required is computed from the vehicle drag, which is a combination of the fuselage drag, blade drag and wing drag (if a fixed wing present). The fuselage equivalent flat-plate area is obtained from gross take-off weight and is given by

$$f = K_f\sqrt{\left(\frac{W}{1000}\right)} \qquad (2)$$

where W is the take-off weight expressed in pounds, and K_f is the empirical constant set to 7.0 for utility helicopters, and between 4.0–5.0 for more streamlined designs (curve fit from Fig. 6.25 (Ref. 14)). Blade drag at the hub is estimated using a corrected disk-averaged force, $F_{x,H}$, as

$$F_{x,H} = N_\mathrm{R}\,\frac{\sigma C_{d_0}}{8}(3.1\mu)\,\rho A(\Omega R)^2 \qquad (3)$$

Mast Drag for Coaxials: For coaxial rotors, the mast drag is folded into the flat-plate area calculations. The mast is assumed to be a cylinder of diameter 7.5% R and a height of 20% R. A fairing with a NACA0020 is assumed. Using a fairing drag coefficient of 0.2 (Ref. 15) yields the mast flat-plate area as

$$f_\mathrm{mast} = 0.003R^2 \qquad (4)$$

Wing Loads: When an asymmetric fixed wing is present, the wing lift fraction is used to compute the contribution of the wing to vertical thrust. The wing lift fraction f_W is a non-dimensional metric between 0 and 1 that represents the fraction of vehicle weight carried by the fixed wing during cruise. The lower limit 0 implies all vertical thrust is provided by the rotor, and 1 implies that the wing carries the entire vehicle weight. Using the vehicle weight generated during each fixed-point iteration, the total wing lift can be computed using the lift fraction. The wing is assumed to operate at its optimum angle of attack for minimum drag, i.e.

$$C_{L_\mathrm{w}} = C_{L_\mathrm{opt}} = \sqrt{\frac{C_{D_0}}{K}} \qquad (5)$$

where $K = 1/(\pi\ \mathrm{AR_{wing}}\ \mathrm{e})$. Therefore, the optimum wing area S_wing is given by

$$S_\mathrm{wing} = \frac{f_\mathrm{W} W_\mathrm{cr}}{0.5\rho V_\infty^2 C_{L_\mathrm{opt}}} \qquad (6)$$

Subsequently, the wing drag D_wing is

$$
\begin{aligned}
D_\mathrm{wing} &= 0.5\rho V_\infty^2 S_\mathrm{wing}(KC_{L_\mathrm{opt}}^2 + C_{D_{0w}}) \\
&= 0.5\rho V_\infty^2 S_\mathrm{wing}(2C_{D_{0w}}) \qquad (7)
\end{aligned}
$$

V_∞ is the forward flight speed, $C_{d_{0W}}$ is the mean drag profile coefficient of the wing and e is the Oswald's efficiency factor. Using the aspect ratio of the wing, $\mathrm{AR_{wing}}$, the wing span, b_wing, and mean wing chord, c_wing are computed as

$$
\begin{aligned}
b_\mathrm{wing} &= \sqrt{\mathrm{AR_{wing}}\ \mathrm{S_{wing}}} \qquad (8) \\
c_\mathrm{wing} &= S_\mathrm{wing}/b_\mathrm{wing} \qquad (9)
\end{aligned}
$$

Therefore, from Eqs. 2, 3, 4 and 7, the total drag is given by

$$D = \frac{1}{2}\rho V_\infty^2(f + f_\mathrm{mast}) + F_{x,H} + D_\mathrm{wing} \qquad (10)$$

Rotor Shaft Tilt in Cruise: To compute rotor induced power, an estimate of the shaft tilt is necessary for use in the uniform inflow iteration expression, and is given below:

- **Without propeller:** The rotor tip-path-plane must be tilted forward to overcome fuselage and blade drag. Using estimates for total drag (Eq. 10) and mean vehicle weight during cruise, the forward tilt of the tip-path-plane is given by

$$\alpha_{\text{TPP}} = \tan^{-1}\left(\frac{D}{W_{\text{cr}}}\right) \tag{11}$$

where D is the drag on the vehicle and W_{cr} is the weight of the vehicle during cruise. The rotor(s) each produce a thrust (assuming no interference) given by

$$T = \frac{1}{N_{\text{R}}}\sqrt{(f_{\text{R}} W_{\text{cr}})^2 + D^2} \tag{12}$$

where f_{R} represents the rotor thrust fraction, i.e., contribution from the rotor(s) to vertical thrust.

- **With propeller:** The rotor tip-path-plane is assumed to be tilted back by 0.5°, so that the thrust vector is dominantly used to counteract gravity. The aft tilt produces a small upwash to aid this thrust generation, i.e.,

$$\alpha_{\text{TPP}} = -0.5^\circ \tag{13}$$

The thrust from each rotor is computed (assuming no interference in cruise) as

$$T = \frac{W_{\text{cr}}}{N_{\text{R}}} f_{\text{R}} \tag{14}$$

Since a small component of the thrust may produce additional hub drag, Eq. 10 is modified to include the component of rotor shaft thrust along the free-stream velocity direction. The total propeller thrust is then given by

$$T_{\text{prop}} = \frac{1}{2}\rho V_\infty^2 f + F_{x,H} + D_{\text{wing}} - N_{\text{R}} T \sin\alpha_{\text{TPP}} \tag{15}$$

The propeller power is estimated from the required thrust, cruise speed and propulsive efficiency as

$$P_{\text{prop}} = \frac{T_{\text{prop}} V_\infty}{\eta_{\text{P}}} \tag{16}$$

When a propeller is present, Eqn. 7 is substituted in Eqn. 15 for calculating the portion of propeller thrust needed to overcome wing drag. When a propeller is not present, Eqn. 7 is substituted in Eqn. 10 to calculate the forward component of rotor thrust.

Rotor Power in Cruise: In high-speed cruise, a tip Mach number limit is imposed by altering the rotor RPM so that

$$\Omega_{\text{cr}} R \leq M_{\text{lim}} a_{\text{cr}} - V_\infty \tag{17}$$

Total inflow for all rotors operating in edgewise flight is obtained through fixed-point iterations for the inflow equation as derived by Glauert (Refs. 16, 17)

$$\lambda = \mu \tan\alpha_{\text{TPP}} + \frac{C_{\text{T}}}{2\sqrt{\mu^2+\lambda^2}} \tag{18}$$

The total inflow ratio, obtained at the end of convergence, is used to calculate the total induced power of all rotors, $P_{\text{i,cr}}$ as

$$P_{\text{i,cr}} = N_{\text{R}}\, \kappa_{\text{C}}\, C_{\text{T}} \lambda\, \rho A (\Omega_{\text{cr}} R)^3 \tag{19}$$

The profile power, $P_{\text{o,cr}}$, needed to rotate the blades and overcome torque due to airfoil section drag in edgewise flight is given by

$$P_{\text{o,cr}} = N_{\text{R}} \frac{\sigma C_{d_0}}{8}(1+1.55\mu^2)\rho A (\Omega_{\text{cr}} R)^3 \tag{20}$$

The total mechanical power , P_{total}, needed to turn the rotor(s) and propeller is then given by

$$P_{\text{total}} = P_{\text{i,cr}} + P_{\text{o,cr}} + P_{\text{prop}} \tag{21}$$

Engine Installed Power The transmission output power is the sum of the power required to rotate the main rotor(s), tail rotor and propeller (if present). Transmission and engine air intake efficiencies, together with temperature/altitude compensations are applied to evaluate to the engine installed power in each mission segment. The maximum installed power and maximum torque are used in the AFDD/NDARC empty weight models to estimate the empty weight contributions from the drive system and air induction groups.

Practical Limits The rotor power calculations in Eqns. 1 and 21 do not take into account local effects like airfoil static stall and advancing blade stresses. Therefore, depending on the choice of input variables (rotor solidity, tip speed and disk loading) the simplified performance calculations will fail to identify designs which are not practical. To filter out designs which require unrealistic values of rotor thrust, two simple thresholds are set to identify unrealistic configurations:

- **Hover blade loading:** When the hover blade loading coefficient C_{T}/σ is above 0.13, the mean operating lift coefficient of the rotor sections is 0.78. Depending on the twist and chord distribution of the rotor sections, certain sections may operate close to stall, leaving little margin for maneuvers or gust tolerance. Therefore, designs that exceed this threshold are discarded.

- **Lift offset:** Rotor lift offset is a non-dimensional metric that represents the lateral bias of average vertical thrust towards the advancing side with respect to the shaft. For a coaxial system, individual rotors may be trimmed to the same lift offset, producing mutually canceling hub rolling moments. For the asymmetric compound design, the lift offset is obtained from the body rolling moment balance equation as

$$L_{\text{off}} = 0.5\, \frac{b_{\text{wing}}}{R}\, \frac{f_{\text{W}}}{1-f_{\text{W}}} \tag{22}$$

The rotor hub rolling moment is then given as

$$L_{\text{HUB}} = L_{\text{off}} R T \tag{23}$$

Where T is each rotor's thrust, given by Eqn. 12 when no propeller is present, and Eqn. 14 when a pusher propeller is included in the design.

It can be shown from aerodynamic considerations (Appendix A) that, based on qualifying assumptions, the lift offset ranges from 0.125 $\mu^3/(1\text{-}0.25\mu^2)$ to $4/3\pi$, with an expected value of $4\mu^3/(3\ \pi\ (1\text{-}0.5\mu^2))$. For the current mission, the cruise advance ratio is approximately 0.75, setting the limits at 0.061 and 0.42, with an expected value of 0.125.

A rotor with a lift-offset greater than 0.5 is required to produce most of its thrust from the outboard sections on advancing blades, resulting in enormous bending loads and associated hub rolling moment. The lower limit 0.1 is set based on the expected value, and 0.5 is set as an inclusive upper bound. These values are inclusive in that they serve to only filter out designs that are clearly infeasible for high advance ratio flight.

With impractical designs weeded out based on hover blade loading and lift offset (for the asymmetric compound), the configurations that "pass" this test are resized based on power predictions from the comprehensive analysis.

Comprehensive Analysis

An in-house comprehensive structural dynamics (CSD) solver was developed at the Alfred Gessow Rotorcraft Center at the University of Maryland based on a doctoral dissertation (Ref. 18), which was also used in CFD-CSD coupling studies (Ref. 19). The CSD solver is used to model the rotor aerodynamics. Blade section aerodynamic forces are obtained using table look-up for Mach number and angle of attack. The inflow calculation can be performed either using the Peters–He dynamic inflow model (Ref. 20) or the Maryland Free-vortex Wake model (MFW) (Ref. 21). When the free wake model is used, alternate updates of wake geometry and trim controls are performed until the rotor swashplate inputs converge across fixed-point iterations.

Power Calculation with Comprehensive Analysis: The comprehensive analysis code is used to evaluated rotor power requirements in cruise, i.e., Eqs. 19 and 20 is replaced by a call to a blade element model. The high-fidelity code is executed in wind-tunnel trim mode, and the collective and cyclics are iteratively adjusted to match target rotor thrust, required rolling moment (obtained from Eqn. 23) and zero net hub pitching moment. Shaft tilt is set to different values based on whether a propeller is present, as given by Eqs. 11 and 13. Blade motions for the cases considered are neglected, since the flap and twist of stiff blades are not expected to have first-order effects on performance. Rotor disk loading and take-off weight are used to prescribe the radius, and the tip speed is used to set the RPM. A uniform chord distribution is prescribed based on blade aspect ratio with 15% root cut-out. The SC1095 airfoil tables are used to compute sectional lift and drag coefficients for various combinations of angle of attack and Mach number.

Once wind-tunnel trim is achieved, the hub drag $F_{x,H}$ and shaft power P_{cr} are extracted from the outputs and used to directly replace the values calculated by Eqs. 3, 19 and 20 respectively.

RESULTS

This section is subdivided into two parts. In the first part, the simple reduced order model (ROM) with empirical corrections is validated and used to infer trends in the empty weight, and to evaluate the merits of the asymmetric design relative to a thrust-augmented coaxial configuration. A focus range for design with comprehensive analysis in the loop is identified to resolve finer details of the design, the results of which are presented in the second part. The comprehensive analysis is used to evaluate rotor power with the aerodynamics resolved at a more fundamental blade element level for the asymmetric compound configuration, and trend differences with the ROM are outlined. A representative mission was chosen for the evaluation of the designs and the mission parameters chosen to size the vehicle are given in Table 3 below:

Mission parameter	Value	Units
Atmosphere	ISA + 5	°C
Hover altitude	2000	meters
Cruise altitude	1000	meters
Hover duration	5	minutes
Cruise speed	200, 240	knots
Payload	2000	kg
Range	450	n.mi

Table 3. Mission requirements

Test Cases for Sizing Analysis

Validation of the HYDRA framework, i.e., using the ROM and the CSD code (with linear inflow), is presented in the following section. The code suite was used to predict the empty weight, installed power and rotor geometry based on available design inputs for the UH-60L, CH-53E, S-97 and UH-1D. It was observed that both the ROM and CSD were able to predict the vehicle parameters within 5% for most parameters.

The results of the sizing code for three production helicopters (light, medium and heavy) and one coaxial compound configuration are shown in Table 4. Two different performance models are used for the vehicles : the energy method based equations with power factors, and comprehensive analysis with rectangular blades.

Part I: Reduced Order Model

The results presented in this section utilize the reduced order model (ROM) which features simple equations for power based on energy relation. Design configuration studies are presented for the asymmetric compound and the thrust augmented coaxial rotor.

UH-60L

Payload, lb	2,645		
Range, nmi	621		
Cruise speed, knots	150		
Solidity	0.082		
Parameter	Reference	ROM	CSD
Empty weight, lb	10,624	10,758	10,830
Rotor diameter, ft	53.666	54.740	54.980
Installed power, hp	3,780	3,995	4,011

CH-53E

Payload, lb	29,982		
Range, nmi	195		
Cruise speed, knots	100		
Solidity	0.1		
Parameter	Reference	ROM	CSD
Empty weight, lb	33,226	35,364	35,364
Rotor diameter, ft	79.0	82.9	82.9
Installed power, hp	13,140	13,622	13,622

S-97

Payload, lb	2,866		
Range, nmi	308		
Cruise speed, knots	220		
Solidity	0.075		
Parameter	Reference	ROM	CSD
Empty weight, lb	–	6,615	6,982
Rotor diameter, ft	34.0	34.98	35.72
Installed power, hp	2,600	2,580	2,779

UH-1D

Payload, lb	1,760		
Range, nmi	243		
Cruise speed, knots	110		
Solidity	0.05		
Parameter	Reference	ROM	CSD
Empty weight, lb	5,215	4,886	4,859
Rotor diameter, ft	48.0	49.36	49.14
Installed power, hp	1,100	1,213	1,226

ROM: Reduced Order Model
CSD: Comprehensive Analysis

Table 4. Comparison of production specifications vs. design outputs using reduced order model and CSD codes

200 knots Cruise: Design Trends

The dominant driving parameters are identified using sweeps over the design space, as given in Table 1, a total of over 200,000 potential designs. In the present study, the most acceptable design was the one that consumed the minimum amount of fuel to complete the specified mission. Of all the configurations investigated, the vehicle specifications for the minimum fuel consumed are given in Table 5. These configurations ("potential designs") were obtained by filtering out converged designs based on both hover blade loading C_T/σ and cruise lift offset. Rotor lift offset is restricted to values from 0.15 to 0.4 (see Appendix A for detailed explanation). The difference between the rotor configurations lie only in the number of blades. Each of the design variables were perturbed around the potential design to identify the sensitivity of the design variable and their roles are highlighted in the following section.

Wing Design Variables

The variables of interest in this section are the wing aspect ratio and the lift fraction, i.e., amount of total lift of the vehicle carried by the wing. **Wing aspect ratio** primarily affects the induced drag and the empty weight of the wing. A value of 9.0 for three, four and five-bladed designs and 7.0 for the six-bladed configuration results in minimum fuel consumption. While the selection process for the "best" design chooses the configuration with the least fuel weight required, the sensitivity of the final vehicle dimensions to variations in wing aspect ratio is very small. Indeed, the top ten designs, ranked by fuel weight, feature all wing aspect ratios from 4 to 10 with all other parameters as given in Table 5. The **wing lift fraction** directly influences rotor lift offset to maintain the rolling moment balance. Figure 3 shows the variation in rotor lift offset as a function of the lift fraction for different number of rotor blades. When the wing is required to carry additional thrust, the rolling moment exerted on the body increases. To counter the wing rolling moment, the rotor was observed to trim with and increased lift offset. If the wing span is restricted to fit within the rotor disk (a restriction placed for practical concerns), then the configurations with minimum fuel consumption, for various numbers of rotor blades, all have an aspect ratio of 7.0.

Rotor Design Variables

The variables of interest that relate to rotor design are the the rotor solidity, disk-loading and the number of blades. Note that the rotational frequency of the rotor is limited based on the maximum tip-speed to prevent compressibility effects on the advancing side in high-speed forward flight. The amount of thrust carried by the rotor is defined by the lift fraction.

Rotor parameter	Value	Units
Disk Loading DL	9	lb/sq.ft
Rotor Solidity σ	0.06	
Number of blades N_b	3 – 6	
Hover tip speed V_{TIP}	240	m/s
Cruise tip Mach limit	0.9	

Wing parameter	Value	Units
Aspect ratio AR	9* (N_b=3,4,5) 7 (N_b = 6)	
Lift fraction f_W	0.3	

Table 5. 200 knots Asymmetric Design: Minimum Fuel

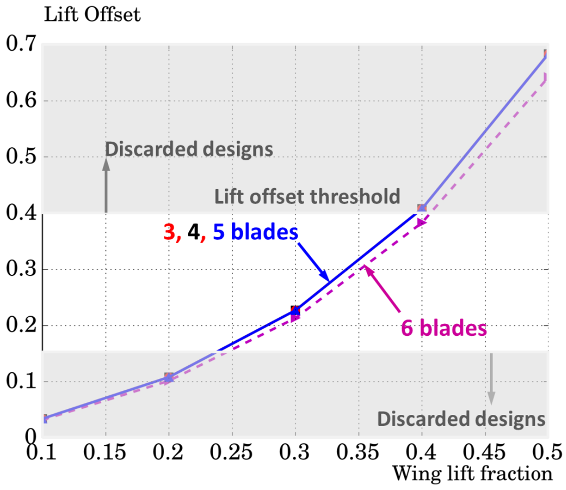

Fig. 3. Variation of rotor lift offset with wing lift

The first parameter investigated is **rotor solidity**. Figure 4 shows the variation of blade loading with increasing rotor solidity. A practical limit is placed on the blade loading coefficient (C_T/σ) of 0.13 and designs that exceed this value are discarded. The observed trend is a decrease in the blade loading for an increase in rotor solidity, all other variables kept the same. For a fixed disk loading and rotor tip speed, larger solidity provides increased hover stall margins, which may be used to operate at higher altitudes or carry heavier payloads for short distances. However, the disadvantage of high solidity designs is a larger empty weight (and therefore, take-off weight). This trend may be derived from the expression for rotor empty weight. Based on production aircraft, the original AFDD00 blade weight model may be rearranged in terms of solidity (instead of aspect ratio) as

$$W_R \approx K\, N_R \frac{R^{2.5}\sigma^{0.75}}{N_b^{0.2}} \tag{24}$$

where K is an empirical constant and other terms retain their usual meaning. Therefore, an increase in the solidity results in an increase in the empty weight of the rotor. The rotor in turn affects the different other empty weights resulting in a total increase of the empty weight of the vehicle. Because most components of vehicle empty weight (listed in Table 2) depend on the take-off weight, it is the rotor weight that drives the sizing and aircraft empty weight. A design with higher solidity results in larger rotor weight, which cascades into larger take-off weight as shown in Fig. 5. Design with lower number of blades have a higher rotor empty weight (see Eq. 24), which is reflected in the higher GTOW for lower blade numbers.

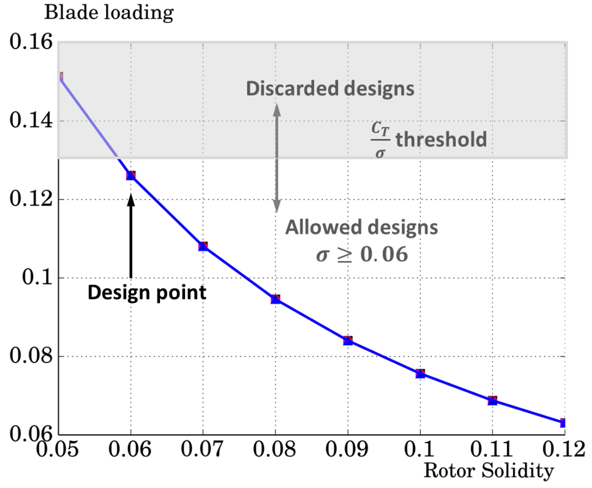

Fig. 4. Variation of blade loading with rotor solidity.

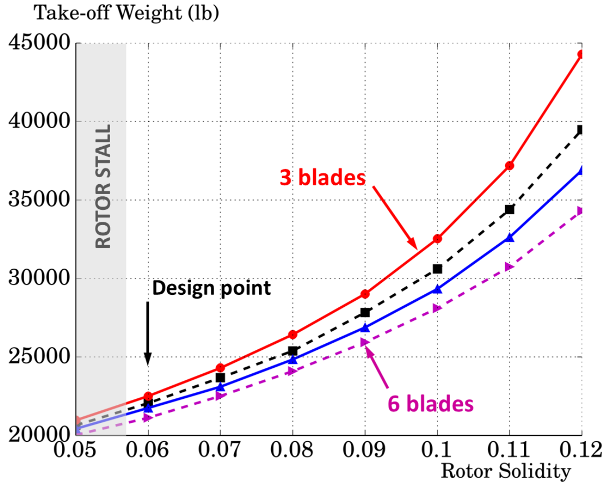

Fig. 5. Variation of take-off weight with rotor solidity.

Disk Loading: A lower disk loading increases the rotor radius for a given take-off weight, shown in Fig. 6, and results in higher hovering efficiencies. However, because empty weight is driven by rotor weight, fixing a very low disk loading results in the classical weight ballooning problem, which manifests as numerical divergence. This weight divergence for low disk loading values is avoided by implementing a maximum cutoff for the rotor radius, and disregarding the prescribed disk loading value. The variation of blade loading with disk loading at fixed rotor solidity is shown in Fig. 7. Designs with disk loading greater than 9.2 lb/sq.ft are discarded based on a blade loading threshold of 0.13.

Take-off weight is also driven by power and torque requirements through the engine and drive system group. For a low-speed design, the installed power is driven by the hover condition. While a larger rotor (lower disk loading) provides improved power loading at a given thrust level, the target thrust itself changes for different rotor sizes. For a high-speed design, propulsive power (through engine and transmission components) drives the empty weight. Rotor induced and profile power requirements also contribute to engine and transmission sizing at high advance ratios. A larger rotor reduces the induced power but greatly increases take-off weight, which subsequently results in increased vehicle drag. For a cruise-efficient design, very high disk loading values result in larger required solidity to avoid airfoil stall, and hover power requirements simultaneously influence engine and transmission sizing. If the disk loading is very low, the diameter drives vehicle weight, drag and installed power as shown in Fig. 8.

Number of Blades: For high rotor solidities, the number of rotor blades has a significant effect on take-off weight. More blades are preferred for a larger rotor diameter or high solidity rotor to reduce the blade weight. For a fixed (low) solidity and disk loading, the blade count does not significantly influence take-off weight and installed power. Changing the number of blades from 3 to 6 decreases the take-off weight and installed power by approximately 5%, rotor radius by 2.5% and fuel required by 4%. The threshold disk loading and solidity values at which C_T/σ exceeds 0.13 are unaffected by the number of blades. The limit on **advancing tip Mach number in cruise** influences rotor power in two ways. Decreasing rotor RPM in cruise reduces rotor profile power, but increases rotor advance ratio and induced power requirements (K_{C}, the induced power factor in cruise, increases (approximately) quadratically with μ (Ref. 12). The trade-off between increasing induced power and decreasing profile power results in a higher desired tip Mach number (0.9) for the simple model without empirical compressibility corrections. For a high-speed design, the **hover tip speed** influences the empty weight through the flight control system and hub groups. Since these components represent a minor contribution to the total weight of a helicopter, the primary influence of hover tip speed is on hover performance and blade loading. The designs with minimum fuel consumption during cruise are those with high hover tip speeds, which complement a low solidity design in avoiding rotor stall. Note that the simple model implemented does not have compressibility corrections, and therefore prefers a lower advance ratio over lower tip speed to minimize induced power in cruise.

Comparison with Coaxial Compound

In this section, 4-bladed designs with minimum fuel consumption are compared between the asymmetric compound and a coaxial compound helicopter for two cruise speeds: 200 knots and 240 knots.

Table 6 compares the final converged design variables for the asymmetric compound and a thrust-augmented coaxial for

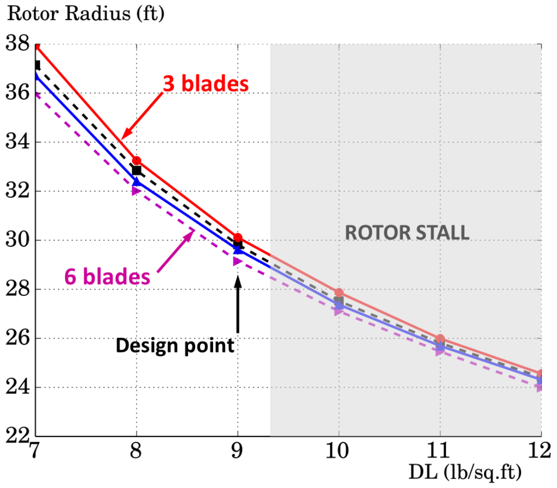

Fig. 6. Variation of rotor radius with disk loading

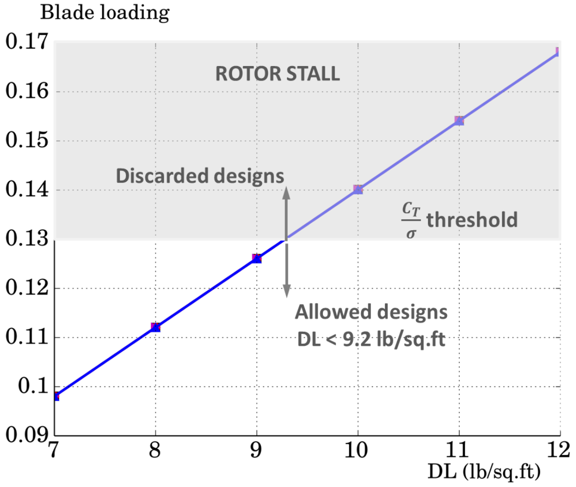

Fig. 7. Variation of blade loading with disk loading

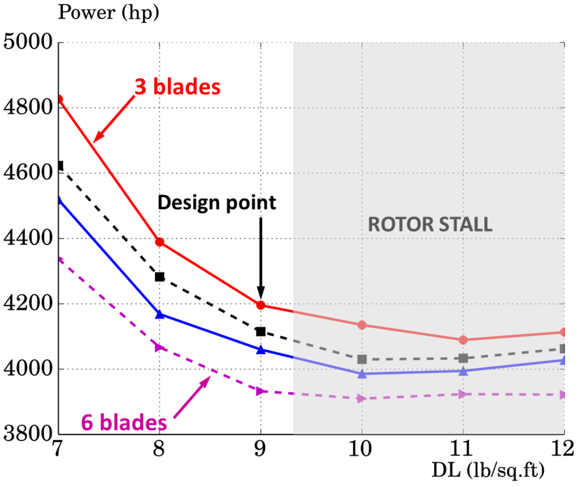

Fig. 8. Variation of installed power with disk loading

a target cruise speed of 200 knots. For this cruise speed, the ROM predicts near-equal performance for the asymmetric compound helicopter and a coaxial design. The coaxial configuration has a lower blade loading coefficient (0.117) than the asymmetric design (0.126). The take-off weights, total disk areas, installed power and fuel required differ by less than 5%. Both designs operate at lift offset values of approximately 0.2 (prescribed for the coaxial configuration). For the asymmetric compound, the wing lift fraction is 0.3, and the span is constrained to fit within the rotor disc. The weight reductions for the coaxial configuration are driven by empty weight reductions obtained from reduced disk loading and solidity. At 200 knots, another coaxial design with disk loading = 9 lb/sq.ft and solidity = 0.06 provides near-identical performance and take-off weight.

Table 7 compares the corresponding design variables and rotor/wing parameters for the two configurations at 240 knots cruise speed. The installed power increases to overcome vehicle drag, driving up empty weight. The fuel required to fly at 240 knots is 60% higher for an asymmetric compound, and 50% higher for a thrust-augmented coaxial design. The simple model predicts a decrease in rotor radius and increased solidity for the 240 knots asymmetric design. The lift fraction carried by the wing is 30%, and wing span is constrained by the rotor radius. Rotor lift offset is 0.21 and insensitive to target airspeed, since it is driven primarily by the wing lift fraction. The empty weight for the two configurations is within 10% at 240 knots.

Rotor parameter	Asymmetric	Coaxial
Number of blades N_b	4	4
Disk Loading *DL*, lb/sq.ft	9	7
Solidity σ	0.06	0.05
Hover tip speed V_{TIP}, m/s	240	240
Cruise tip Mach limit	0.9	0.9
Gross Weight, lbs	21,780	21,738
Fuel Weight, lbs	2,944	2,640
Empty Weight, lbs	15,306	14,697
Installed Power, hp	4,065	3,970
Radius, ft	32.9	23.72
Lift Offset	0.21	0.2
Wing parameter	Value	Units
Aspect ratio *AR*	7	–
Span, ft	29.5	–
Lift fraction f_W	0.3	–

Table 6. 200 knots Design for Minimum Fuel, N$_b$ = 4 blades in Each Rotor for Coaxial

Rotor parameter	Asymmetric	Coaxial
Disk Loading *DL*, lb/sq.ft	12	9
Rotor Solidity σ	0.08	0.06
Hover tip speed V_{TIP}, m/s	240	240
Cruise tip Mach limit	0.9	0.9
Gross Weight, lbs	27,065	24,376
Fuel Weight, lbs	4,838	3,951
Empty Weight, lbs	17,827	16,025
Installed Power, hp	7,017	5,818
Radius, ft	28.6	22.15
Lift Offset	0.21	0.2
Wing parameter	Value	Units
Aspect ratio *AR*	8	–
Span, ft	28.3	–
Lift fraction f_W	0.3	–

Table 7. 240 knots Design for Minimum Fuel, N$_b$ = 4 blades in each Rotor

Quantitative inferences of relative performance benefits between the coaxial and the asymmetric compound can be misleading, as the ROM has inherent assumptions in its formulation that may break down at this flight condition. At this high-speed, the advance ratio is approximately 0.75, where simple models for induced power factors may break down and sizing is driven significantly by cruise power predictions. Therefore, the design sweep was rerun using the CSD solver to evaluate rotor performance. The results of this study are presented in the following section.

Part II: Comprehensive Analysis

In this section, the reduced order models used in the performance routines of the design codes are replaced by comprehensive analysis tools augmented with a linear inflow model or freewake. The design from the Part I are refined and blade level optimization is performed.

Design with Comprehensive Analysis for Performance

The 240 knots designs generated with the reduced order model are compared to the counterparts obtained using comprehensive analysis for performance prediction. This higher fidelity performance module was used to compute rotor power with 0, 5 and 10 degrees of blade geometric twist for the asymmetric compound and thrust augmented coaxial. Both vehicles used 4 blades per rotor.

The asymmetric compound configurations with least fuel consumption are given in Table 8 for 0, 5 and 10 degrees of blade twist. The optimal disk loading and solidity obtained with the comprehensive analysis were very similar to those obtained using the ROM for all blade twist levels investigated. The hover tip speed was sufficiently high to restrict the blade loading coefficient at take-off to 0.13. With compressibility effects now introduced by the airfoil tables, the maximum advancing tip Mach number in cruise was 0.8 for minimum fuel consumption. The ROM has incorporated within it an empirical model for the induced power factor, which is in excess of 4 at $\mu = 0.75$ and over-predicts this rotor induced power requirement in edgewise flight. Therefore, for designs focused on high-speed cruise, the power predictions primarily drive the sizing of the vehicle. Compared to the ROM, the take-off weight for all three twist levels is 11% lower when the comprehensive analysis is included, as shown in Table 7. Installed power and fuel weight required are 16% and 20% lower, respectively, for the comprehensive analysis predictions with linear inflow. The corresponding effect on reduced gross weight is immediately apparent in the predictions of the resulting rotor radius, which is 26 ft (instead of 28.3 ft).

The wing sizing is driven by the permitted rotor lift offset limits and the resolution of wing lift fraction prescribed in the parametric sweeps. As in the case with the ROM, wing aspect ratio is not a driving design parameter for sizing this configuration. The top ten designs feature wing aspect ratios 4 – 8 with only 4% change in fuel required. Wing span is close to 26 ft, with less than 1% difference between the three blade twist levels. The configuration with minimum fuel consumption requires that the wing carry 40% of the total weight, and the corresponding rotor lift offset is 0.31.

The coaxial compound configurations with best fuel consumption are given in Table 9 for 0, 5 and 10 degrees of blade twist, respectively. Hover tip speed and the maximum allowed advancing tip Mach number in cruise are 240 m/s and 0.8 respectively, identical to the asymmetric configuration. The best rotor disk loading and solidity are 16 – 17 lb/sq.ft and 0.14 – 0.16, respectively. The high disk loading is a result of a more compact rotor lowering take-off weight; see Eqn. 24. A high solidity design is required to restrict hover blade loading to acceptable limits. Induced and profile power requirements from the comprehensive analysis are obtained assuming no wake interference at high speeds.

The two configurations, i.e., coaxial and asymmetric compound, fall in the same weight class for the chosen mission and cruise speed. Take-off weight is more sensitive to choice of blade twist, indicating that profile and induced power are key sizing drivers for the coaxial more than the asymmetric compound. The installed power difference between the "best" coaxial and asymmetric compound configurations, when including blade twist, is significant. The high disk loading predicted using CSD performance results in a more compact rotor (16.1 ft vs. 22 ft), higher installed power (+17%) and more fuel (+13%).

With appropriate tuning of the ROM for a limited range of blade loading and advance ratio, the accuracy can be improved. However, this is not a robust solution for incorporating high advance ratio physics into the design process, and predictions may be misleading. This result is evident in the comparisons of fuel required for the coaxial configuration in Tables 7 and 9.

With the ROM, Table 7 indicates that the asymmetric design requires more fuel than the coaxial compound. These findings are in direct contrast to those obtained using the high-fidelity performance model, as shown in Tables 8 and 9. With the high-fidelity performance model, the fuel required to complete the mission is 20% lower for the asymmetric compound than for the coaxial configuration.

Rotor parameter	Untwisted	5 deg	10 deg
Disk Loading DL, lb/sq.ft	13	13	12
Rotor Solidity σ	0.09	0.09	0.08
Hover tip speed V_{TIP}, m/s	240	240	240
Cruise tip Mach limit	0.8	0.8	0.8
Gross Weight, lbs	23,908	23,425	23791
Fuel Weight, lbs	4023	3870	3913
Empty Weight, lbs	15484	15156	15478
Installed Power, hp	5908	5677	5748
Radius, ft	26.03	25.78	27.03
Lift Offset	0.33	0.33	0.32
Wing parameter	Untwisted	5 deg	10 deg
Aspect ratio AR	4	4	4
Span, ft	26.03	25.77	25.96
Lift fraction f_W	0.4	0.4	0.4

Table 8. 240 knots Asymmetric Designs : Min. Fuel, N_b= 4

Rotor parameter	Untwisted	5 deg	10 deg
Disk Loading DL, lb/sq.ft	16	16	17
Rotor Solidity σ	0.16	0.14	0.14
Hover tip speed V_{TIP}, m/s	240	240	240
Cruise tip Mach limit	0.8	0.8	0.8
Gross Weight, lbs	27,962	25,210	24098
Fuel Weight, lbs	5161	4658	4510
Empty Weight, lbs	18401	16151	15188
Installed Power, hp	7767	6900	6725
Radius, ft	17.94	17.03	16.14
Lift Offset	0.27	0.27	0.27

Table 9. 240 knots Coaxial Designs : Min. Fuel, N_b= 4 blades in Each Rotor

To identify physical mechanisms behind the large power penalty for untwisted rotors with lift offset, contour plots of the normal force and chordwise force were generated from the comprehensive analysis for three different twist gradients at a fixed thrust level. Shown in Fig. 9 are contour plots of operating angles of attack and in-plane force (analogous to induced + profile drag) for three different twist levels. The region around the reverse flow bubble is stalled and very similar

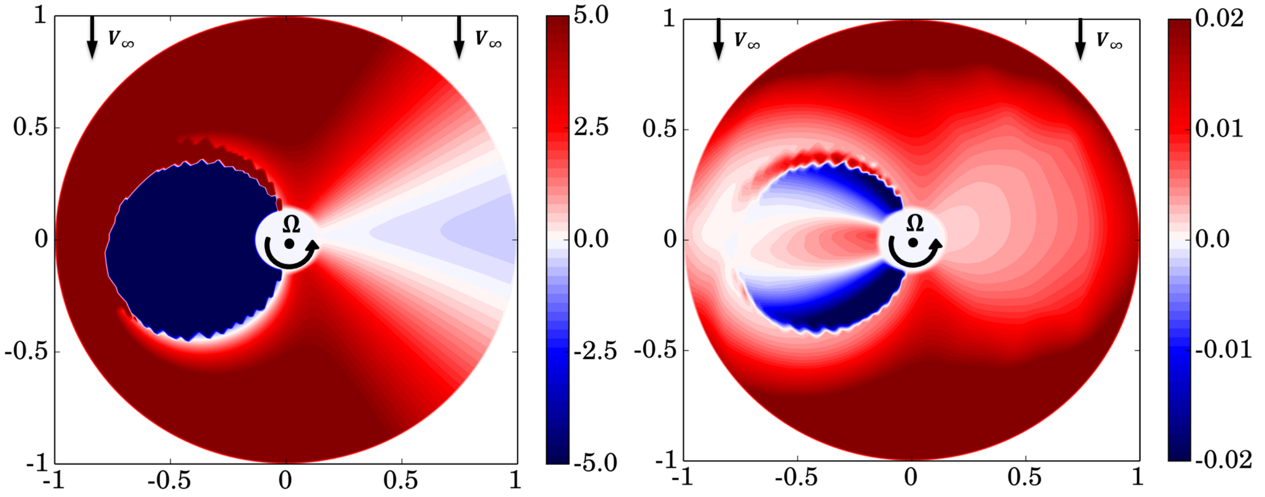

(a) Angle of Attack : Untwisted Rotor

(b) Chordwise Force : Untwisted Rotor

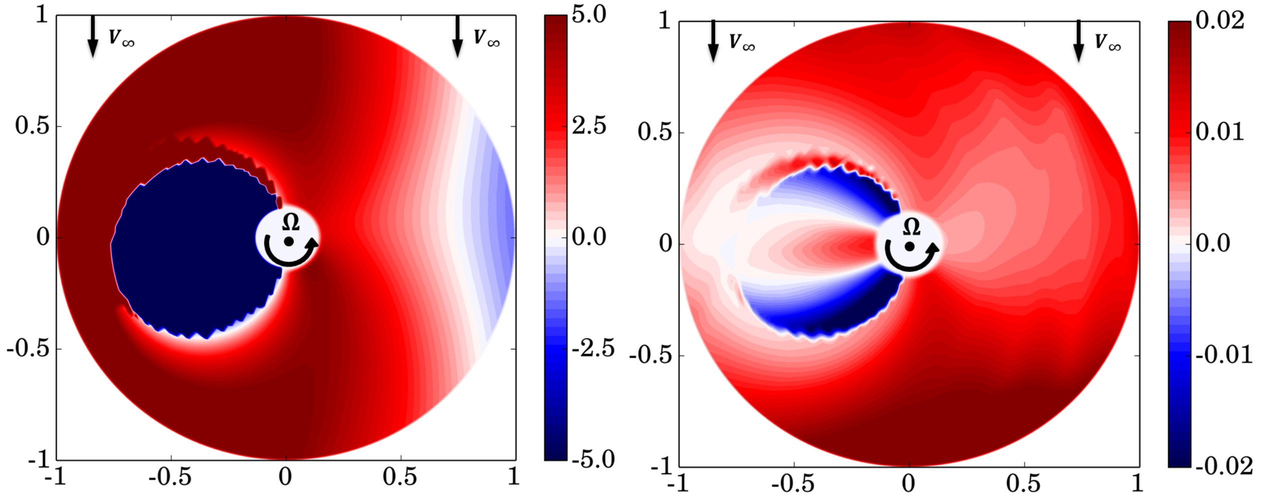

(c) Angle of Attack : θ_{TW}=5 deg

(d) Chordwise Force : θ_{TW}=5 deg

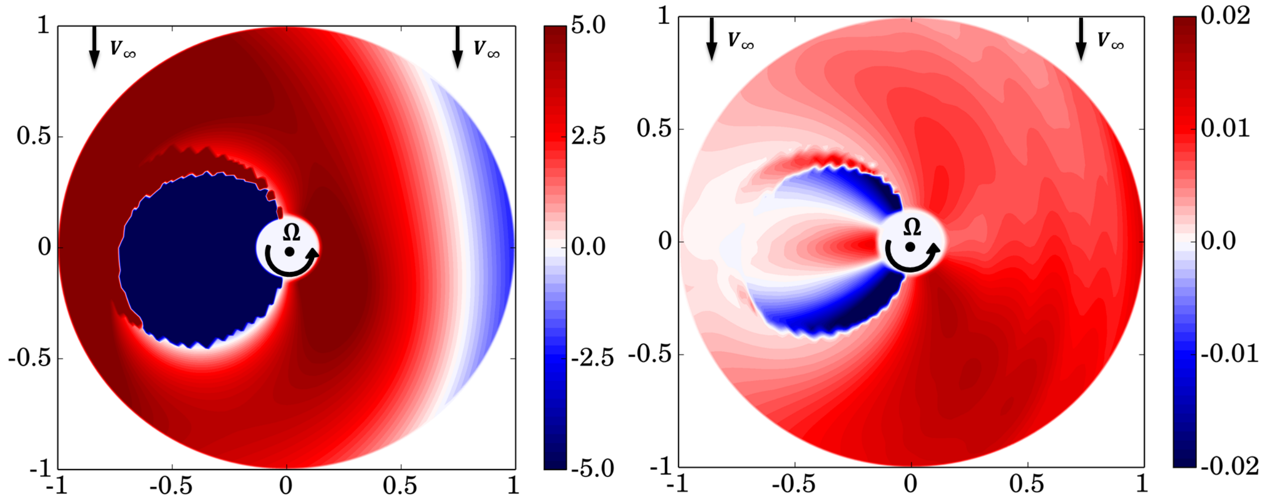

(e) Angle of Attack : θ_{TW}=10 deg

(f) Chordwise Force : θ_{TW}=10 deg

Fig. 9. In-plane and Normal Force Contours for Various Blade Twists

for all three twist configurations considered. Over the fore and aft of the disk, and on the advancing side, the loads are redistributed with different twist levels. For the untwisted blade, the operating angles of attack are in excess of 5 degrees over most of the region between ψ = 120 deg and ψ = 60 deg. The corresponding increase in chordwise force over the fore and aft sections of the disk is evident in Fig. 9(b). As blade twist increases, the operating angles of attack decrease on the advancing side, reducing drag and power consumption.

Fig. 11 shows the variation of rotor thrust for the three twists considered. For untwisted blades, most of the thrust produced at blade tip regions at azimuths around $\psi = 45, 135$ deg. As twist increases, the thrust is redistributed to the region 45 deg $\leq \psi \leq$ 135 deg near the mid span regions. For excessive blade twist, the tip sections experience a slight negative lift. On the retreating side, the region around the reverse flow bubble is essentially unloaded. This study highlights an important design criterion: judicious levels of blade twist may help improve performance for lift-offset rotors at high advance ratios.

Blade Geometry Optimization

The rotor diameter, number of blades, solidity, cruise tip speed and cruise airspeed from Table 8 were frozen. For this stage of the optimization, parametric sweeps of the blade twist and taper are carried out to identify the geometry for minimum cruise power at 240 knots. The corresponding ranges of various design variables are given in Table 10, and a general blade geometry is shown in Fig. 10.

The chord at the bilinear taper junction was set to preserve rotor geometric solidity for each combination of root and tip chord. A total of 7,500 blade designs were evaluated using the linear inflow model and the free wake model separately.

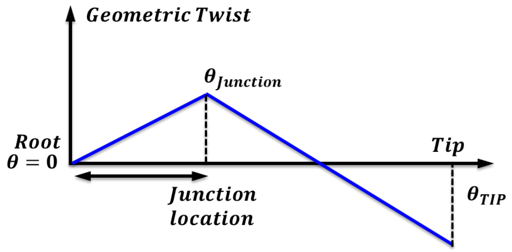

(a) Bilinear Twist

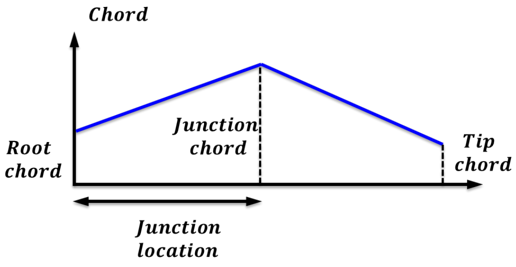

(b) Bilinear Taper

Fig. 10. Rotor Blade Design Parameters

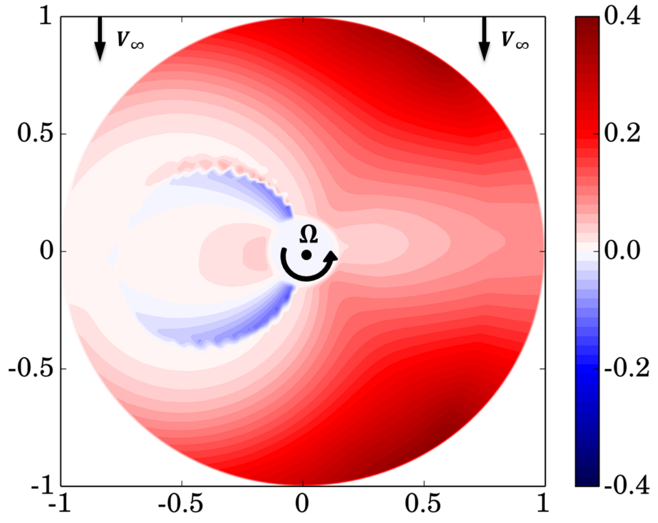

(a) Normal Force Contours : Untwisted Rotor

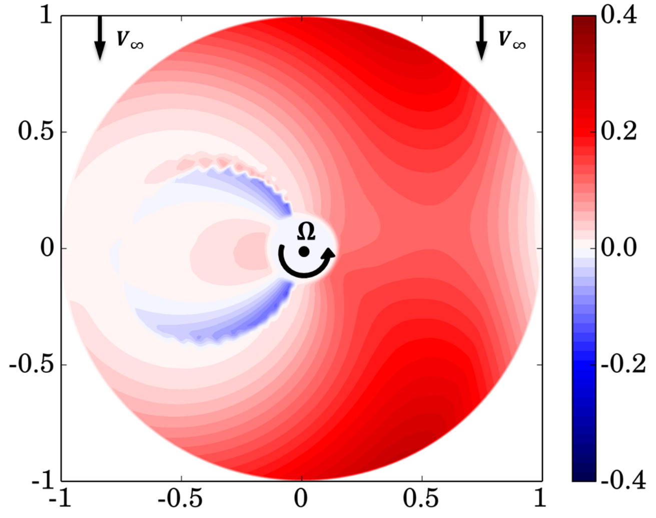

(b) Normal Force Contours :θ_{TW}=5 deg

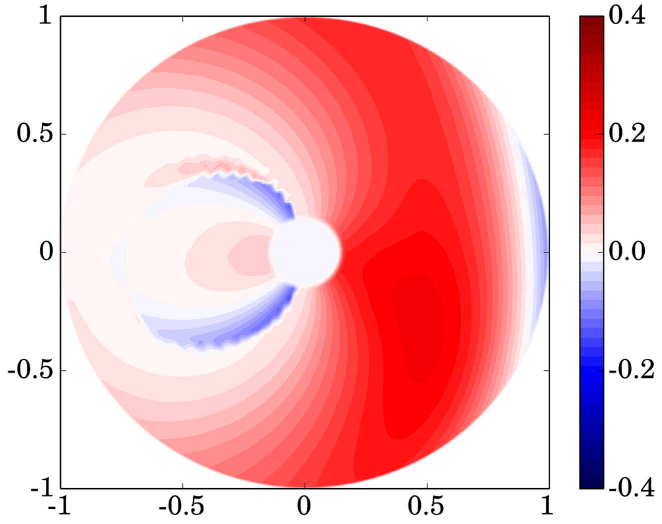

(c) Normal Force Contours :θ_{TW}=10 deg

Fig. 11. Normal Force Contours for Various Blade Twists

Blade Design Parameter	Value
Bilinear Twist Junction	0.4 – 0.8
Twist at Junction (deg)	-10° – 2.5°
Tip Twist (deg)	-12.5° – 0°
Bilinear Taper Junction	0.4 – 0.8
Root Chord / Mean Chord	1 – 1.2
Tip Chord / Mean Chord	0.6 – 1

Table 10. Blade Design Variables for Parametric Sweep

Blade Geometry Parameter	Linear Inflow	Free Wake
Bilinear Twist Junction	0.6	0.7
Twist at Junction (deg)	-5°	-5°
Tip Twist (deg)	-7.5°	-10°
Bilinear Taper Junction	0.5	0.7
Root Chord / Mean Chord	1.2	1.0
Tip Chord / Mean Chord	0.6	0.6

Table 11. Optimum Blade Geometry for 240 knots Cruise, Linear Inflow vs. Free Wake

Blade Geometry	Power (% redn.) Linear Inflow	Power (% redn.) Free Wake
Untwisted	899 hp (0%)	1129 (0%)
Bilinear taper	894 hp (-1%)	1065 (-6%)
10 deg linear twist	781 hp (-13%)	779 (-29%)
Bilinear twist	743 hp (-17%)	772 (-32%)
Optimum	701 hp (-22%)	761 (-33%)

Table 12. Rotor Power Comparison at 240 knots Cruise: Various Blade Geometries; Linear Inflow and Free Wake. Bilinear twist and bilinear taper from Table 10

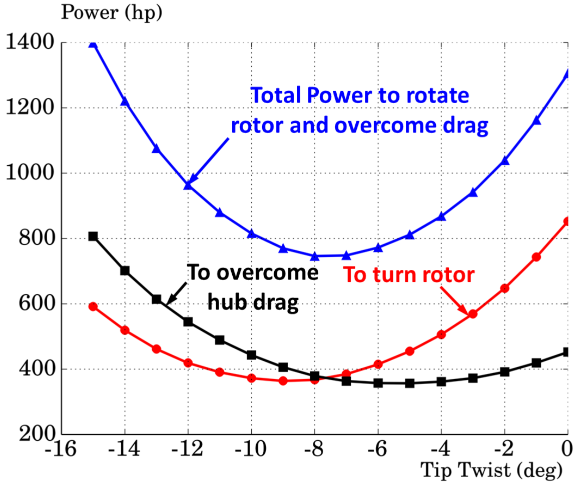

Fig. 12. Effect of Blade Tip Twist on Cruise Rotor Power. Results obtained from Linear Inflow Model

The optimum geometry was identified based on minimum cruise power, and is tabulated in Table 11. All parameters except tip twist are very close to each other. The optimum tip twist predicted using linear inflow is -7.5 deg, while free wake-based analysis predicts -10 deg. The optimum twist distribution based on linear inflow predictions exhibits an inboard gradient of 8.3°/non-dimensional span from 15% (root cut-out) to 60% span, and an outboard gradient of 6.25°/non-dimensional span from 60% span to the tip. This twist distribution, particularly at the tip, is consistent with the results in Figs. 9 and 11. As the blade geometry changes from 0 to 10 degrees of total twist, the advancing tip regions are progressively unloaded and thrust is redistributed to the mid-span locations. Further, the angles of attack over the front and rear of the rotor are such that the in-plane force reduces. However, at 10 degrees of tip twist, the advancing blade tips experience negative lift, resulting in an unfavorable operating condition. Therefore, it is expected that the optimum linear twist may lie between 5 and 10 degrees.

Table 12 shows the comparison of rotor power (induced + profile, including hub drag) required at 240 knots cruise for various blade geometries. The untwisted blades are selected as baselines to emphasize the role of rotor geometry. For the untwisted blade, linear inflow predicts a power of 900 hp, while free wake predicts 25% higher power (1,129 hp). Both methods predict approximately the same power for the respective optima.

Blade tip twist is the key design parameter that significantly affects cruise power. The breakdown of rotor power into that required to turn the shaft, and the additional propeller power needed to overcome hub drag is shown for various tip twists in Fig. 12. Even 10 deg of twist provides significant cruise power savings at 240 knots. Finally, bilinear taper is not as effective as bilinear twist when applied separately. However, simultaneous application of the two results in significant rotor power savings.

Role of Hub Drag at High Forward Speeds At a forward speed of 240 knots (405.3 ft/s), the rotor vertical thrust required is 14,260 lbs, and the rest of the weight is carried by the fixed wing. At this speed, the hub drag is of the order of hundreds of pounds (3% of vertical thrust). For a blade with 10 deg twist and bilinear taper given in Table 10, the shaft power predictions are 315 hp and 314 hp, respectively, using the linear inflow and free wake models. However, the hub drag predictions using the two inflow models are 482 lb and 591 lb. The two aerodynamic models predict the same shaft power but different hub drag values. This difference is not significant in comparison to the engine installed power. The difference in hub drag predictions is responsible for the different optimal blade geometries for the two inflow models. However, the difference is not large enough to impact the sizing of this helicopter.

In the following section, the optimum blade geometry is used to generate the power curve for the aircraft in steady level forward flight at flight speeds between 0 (hover) and 240 knots (cruise). The linear inflow model predictions are compared to those obtained using a free wake analysis. Vehicle force balance in the longitudinal plane and about the body roll axis are used to determine wind-tunnel trim targets for the rotor. The hub X-force is used together with the wing drag and airframe drag to compute propeller power in forward flight. The wing lift coefficient is assumed to be constant throughout, and equal to the optimal value given in Eqn. 5. This assumption is consistent with zero wake interference (valid at high speeds) and a constant wing mounting angle.

Power Curve: Figure 13 shows the variation of rotor power, propeller power and total power required for various flight speeds, as predicted using the free wake and linear inflow models. Propeller power is near-identical between the two models, since it is dominantly driven by rotor drag, vehicle drag and wing drag. Since rotor drag predictions do not differ appreciably between the two models, propeller power agreement is similarly good. At the design cruise speed, both models collapse to the same prediction value. The choice of inflow model affects the hub drag, which then cascades into propeller power. While rotor power is different by as much as 500 hp, the disagreement in total power is within 150 hp. For this particular design, the cruise power and hover power are equal, resulting in maximum use of engine power.

In summary, rotor aerodynamics at high advance ratios results in significant breakdown of underlying assumptions used in the simplified performance models. While implementation of tuned induced power factors as table look-up functions of thrust and flight conditions may circumvent the issue temporarily, including the comprehensive analysis within the design iterations as a higher-fidelity alternative avoids the problem altogether. This capability presents an option to the designer to obtain rotor performance using detailed physics-based models with fewer underlying assumptions.

CONCLUSIONS

Sizing studies and rotor blade-level optimizations were performed in the design of a high-speed asymmetric compound (half wing with a lift-offset rotor) capable of performing a similar mission as a full scale conventional single main rotor helicopter. A numerical framework (HYDRA) was developed, which consists of a sizing procedure with options to use either a reduced order model or comprehensive analysis for performance calculations. Based on this framework, a successful asymmetric compound design was obtained that utilized with the wing and rotor operating under practical aerodynamic limits. Furthermore, this compound design was compared to a coaxial rotor and it was shown that the asymmetric compound requires lower installed power and fuel weight to perform the same mission as the sized-coaxial vehicle.

The following specific conclusions were drawn from this study

1. The multi-fidelity framework allows a wide exploration of the design space using a reduced order model before down-selecting designs that are reevaluated and optimized using the higher-fidelity comprehensive analysis either with a linear inflow model or freewake. The entire procedure converges to a practical design within two hours, including the parameter search for the best blade geometry using free wake.

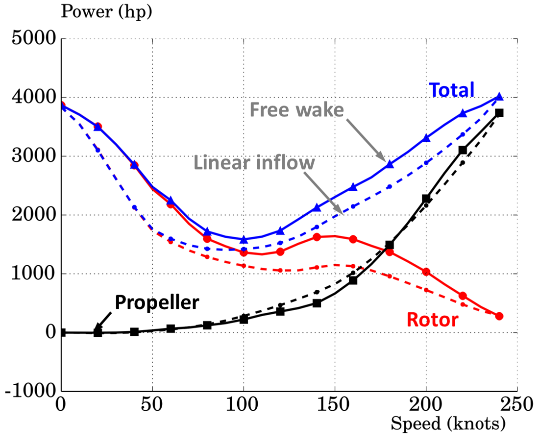

(a) Power Curve

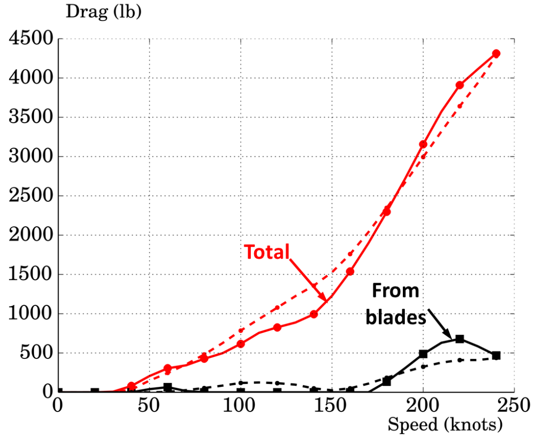

(b) Drag

Fig. 13. Power and Drag Breakdown at Various Flight Speeds: Linear Inflow (– –) vs. Free Wake (–)

2. Simple equations tend to reply on empirical trends to capture physical phenomenon such as the induced power factor, which tend to erroneously over-predict or under-predict performance (these factors are not necessary tuned to extreme flight conditions). The performance of the rotor was better predicted using comprehensive analysis in the design loop.

3. A nominal amount of blade twist was found to be beneficial for improving the performance of the high advance ratio lift-offset rotor considered. The underlying mechanism for power reduction is a redistribution of the airloads over the rotor disk, and reduction of operating angles of attack (and hence drag) over the nose and tail.

4. The rotor radius drives the empty weight through a cascading mechanism by affecting other weight groups. The installed power sensitivity to blade geometric has a mea-

surably significant outcome on the final design and cruise power requirements. Blade taper had a secondary effect on the design considered, as in the present study, the advancing tip Mach number was constrained to 0.8.

5. At these high forward-flight speeds, the difference in the inflow distribution between a linear inflow model and freewake was found to be negligible. The wake was predominantly blown away behind the rotor, resulting in near-identical rotor shaft torque for the same operating condition. The main difference between a free wake model and a simple inflow model is evident in the hub longitudinal force due to blade drag.

APPENDICES

Appendix A: Lift Offset from Disk Loading

This section provides estimates for the variation of rotor lift offset with advance ratio, based on the assumption that the rotor disk is split into multiple regions, each of which experiences uniform loading per unit area with different intensities. The rotor disk is subdivided as shown in Fig. 14 into the following regions:

- The outer ring of the rotor disk that is always in attached flow. The disk loading is l_1. The equation describing this region is $x \geq \mu$.
- The portion of the advancing side, minus the outer ring: flow is fully attached. The disk loading is l_2. The equation describing this region is $x \leq \mu$, $0 \leq \psi \leq \pi$.
- The reverse flow "bubble": rotor blade sections experience relative velocity from the trailing edge to the leading edge. The disk loading is l_3. The equation describing this region is $x + \mu \sin\psi \leq 0$
- The remainder of the rotor disk: retreating side excluding the reverse flow region and outer band. The disk loading is l_4. The equation describing this region is $x + \mu\sin\psi \geq 0, x \leq \mu, \pi \leq \psi \leq 2\pi$.

The total thrust generated by the rotor is

$$T = \pi R^2(1-\mu^2)l_1 + 0.5\pi\mu^2 R^2(l_2+l_4) - \pi R^2(l_4-l_3)\frac{\mu^2}{4} \tag{25}$$

The total hub rolling moment is

$$L_{\text{HUB}} = 0.5\pi R^2\mu^2\frac{4\mu R}{3\pi}(l_2-l_4) + \pi R^3(l_4-l_3)\frac{\mu^3}{8} \tag{26}$$

The general expression for lift offset is

$$L_{off} = \frac{\frac{4\mu^3}{6\pi}(l_2-l_4) - 0.125\mu^3(l_3-l_4)}{0.5(l_2+l_4)\mu^2 + 0.25(l_3-l_4)\mu^2 + (1-\mu^2)l_1} \tag{27}$$

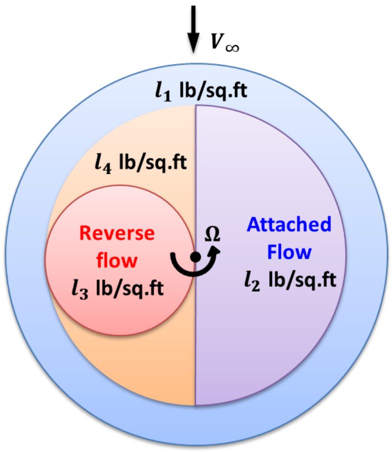

Fig. 14. Subdivision of Rotor Disk Areas

If the disk loading is zero in the reverse flow bubble and uniform in all other regions, then the lower bound of lift offset is

$$L_{off,1} = \frac{0.125\mu^3}{1-0.25\mu^2} \tag{28}$$

If the disk loading is zero on the retreating side, then the upper bound of lift offset is

$$L_{off,2} = \frac{8}{6\pi} \approx 0.424 \tag{29}$$

The upper bound is not a function of advance ratio, since it is simply the centroid of the half-circle.

If the inner ring on the retreating side does not produce any lift and loading is uniform everywhere else, i.e $l_3 = l_4 = 0$ and $l_1 = l_2$, then the lift offset is

$$L_{off,3} = \frac{4\mu^3}{6\pi(1-0.5\mu^2)} \tag{30}$$

Appendix B: Lift Offset from Blade Element Analysis

Using blade element theory, the lift offset of a high advance ratio rotor may be estimated using the following assumption: on the advancing and retreating sides, all blade sections operate at a lift coefficient given by C_{l_A} and C_{l_R} respectively. The dynamic pressure is computed using the tangential and radial velocities; disk tilt and blade motions are ignored. Under these assumptions, the total rotor thrust simplifies to

$$\frac{C_T}{\sigma} = \frac{1}{4}\left[\left(C_{l_\text{A}} + C_{l_\text{R}}\right)\left(\frac{1}{3}+\mu^2\right) + \left(C_{l_\text{A}} - C_{l_\text{R}}\right)\frac{2\mu}{\pi}\right] \tag{31}$$

The rotor rolling moment is given by

$$\frac{C_L}{\sigma} = \frac{1}{4}\left[\left(C_{l_\text{A}} - C_{l_\text{R}}\right)\frac{1}{\pi}\left(\frac{1}{2}+\mu^2\right) + \left(C_{l_\text{A}} + C_{l_\text{R}}\right)\frac{\mu}{3}\right] \tag{32}$$

Defining the ratio

$$r_\text{L} \overset{\text{def}}{=} \frac{1 - \frac{C_{l_\text{R}}}{C_{l_\text{A}}}}{1 + \frac{C_{l_\text{R}}}{C_{l_\text{A}}}} \tag{33}$$

The lift offset may be written as

$$L_{off} = \frac{r_{\mathrm{L}}(0.5+\mu^2)+\frac{\pi\mu}{3}}{2\mu r_{\mathrm{L}}+\pi\left(\frac{1}{3}+\mu^2\right)} \tag{34}$$

When the retreating side carries no lift, the ratio r_{L} collapses to unity, and the upper bound of lift offset is

$$L_{off,max} = \frac{0.5+\mu^2+\frac{\pi\mu}{3}}{2\mu+\pi\left(\frac{1}{3}+\mu^2\right)} \tag{35}$$

Numerical values of this upper limit of lift offset vary from 0.45 ($\mu = 0.5$) to 0.39 ($\mu = 1.5$). This result is also close in value to that obtained in Appendix A, using a uniform disk loading assumption.

If the advancing and retreating sides operate at the same lift coefficient, then the lift offset is

$$L_{off,est} = \frac{\mu}{1+3\mu^2} \tag{36}$$

Numerical values of this lift offset estimate range from 0.29 (μ=0.52) to 0.25 ($\mu = 1.0$).

Appendix C: Wing Lift Fraction and Lift Offset

For the asymmetric compound, rotor thrust and wing lift are related through vehicle weight, rolling moment balance and cruise lift share. Therefore, the rotor lift offset may be expressed in terms of wing span, rotor radius and wing lift fraction as

$$L_{off} = \frac{f_{\mathrm{W}}W(0.5b)}{(1-f_{\mathrm{W}})WR} = \frac{f_{\mathrm{W}}}{1-f_{\mathrm{W}}}\frac{b}{2R}$$

After substituting for the wing dimensions from expressions given in the Methodology section, the lift offset expression simplifies to the following combination of non-dimensional parameters

$$L_{off} = \frac{f_{\mathrm{W}}^{1.5}}{1-f_{\mathrm{W}}}\frac{\lambda_h}{\mu}\frac{\Omega_h}{\Omega_{\mathrm{cr}}}\sqrt{\frac{1}{e}\frac{C_{L_{\mathrm{opt}}}}{C_{D_{0w}}}} \tag{37}$$

In terms of design parameters, the lift offset is

$$L_{off} = \frac{f_{\mathrm{W}}^{1.5}}{1-f_{\mathrm{W}}}\sqrt{\frac{0.5DL}{\rho V_\infty^2}\frac{1}{e}\frac{C_{L_{\mathrm{opt}}}}{C_{D_{0w}}}} \tag{38}$$

The above expression may also be used to quickly eliminate infeasible combinations of wing lift fraction and rotor disk loading for a given cruise speed.

REFERENCES

[1] Johnson, W., "A History of Rotorcraft Comprehensive Analyses," NASA TP-2012-216012, Ames Research Center, Moffett Field, CA, April 2012.

[2] Yeo, H., and Johnson, W. "Aeromechanics Analysis of a Heavy Lift Slowed-Rotor Compound Helicopter," *Journal of Aircraft*, Vol. 44, No. 2, March–April 2007.

[3] Yeo, H., Sinsay, J.D., and Acree, C.W., Jr., "Blade Loading Criteria for Heavy Lift Tiltrotor Design," American Helicopter Society Southwest Region Technical Specialists' Meeting on Next Generation Vertical Lift Technologies, Dallas, TX, October 2008.

[4] Vu, N. A., Lee, Y-J., and Kim, S., "Configuration Design and Optimization Study of a Compound Gyroplane," *Aircraft Engineering and Aerospace Technology*, Vol. 83, No. 6, pp. 420–428, 2011.

[5] Avera, M., Kang, h., and Singh, R., "Comprehensive Rotorcraft Analysis for Preliminary Design and Optimization," Proceedings of the 71st Annual Forum of the American Helicopter Society, Virginia Beach, VA, May 5–7, 2015.

[6] David, C.V., "Heliplane", U.S. Patent No. 4,730,795. 15 Mar. 1988.

[7] Cai, G., Dias, J., and Seneviratne, L., "A Survey of Small-Scale Unmanned Aerial Vehicles: Recent Advances and Future Development Trends", *Unmanned Systems*, Vol. 2., No. 2, 2004, pp. 1–25.

[8] Sartorius, S., "A Tool for Rotorcraft Pre-Design Sizing," Proceedings of the 67th Annual Forum of the American Helicopter Society, Virginia Beach, VA, May 3–5, 2011.

[9] Cumbreras, P. R., and Sartorius, S., "Feasibility Study of a Novel Asymmetric Rotorcraft Configuration: Single-Rotor Advancing Blade Concept," Presented at the 2013 International Powered Lift Conference, AIAA Aviation, Los Angeles, CA, August 12–14, 2013.

[10] Tishchenko, M. N., and Nagaraj, V. T., "ENAE634 Helicopter Design Lecture Notes," University of Maryland, College Park, 2010.

[11] HeliX, 30th Annual American Helicopter Society, Student Design Competition, University of Maryland, College Park, 2012.

[12] Johnson, W., "NDARC - NASA Design and Analysis of Rotorcraft Validation and Demonstration," AHS Aeromechanics Specialists Meeting, San Francisco, CA, Jan. 20–22, 2008.

[13] Moodie, A.M., and Yeo, H., "Design of a Cruise-Efficient Compound Helicopter," *Journal of the American Helicopter Society*, Vol. 57, No. 3, pp. 1–11, 2012.

[14] Leishman, J. G., "Principles of Helicopter Aerodynamics," Second Edition, Cambridge University Press, 2006.

[15] Miklosovic, D.S., Murray, M.M. and Laurens, E.H., "Experimental Evaluation of Sinusoidal Leading Edges", *Journal of Aircraft*, Vol. 44, No. 4, July-August 2007, pp. 1404–1407.

[16] Glauert, H., "On the Horizontal Flight of a Helicopter," ARC R & M 1157, 1928.

[17] Glauert, H., "Airplane Propellers," In Division L of *Aerodynamic Thoery,* ed. W. F. Durand, Springer Verlag, Berlin, Germany, 1935.

[18] Sridharan, A., Simulation Modeling of Flight Dynamics, Control and Trajectory Optimization of Rotorcraft Towing Submerged Loads," Ph.D. Dissertation, Department of Aerospace Engineering, University of Maryland at College Park, 2014.

[19] Passe, B., Sridharan, A. and Baeder, J.D., "Computational Investigation of Coaxial Rotor Interactional Aerodynamics in Steady Forward Flight", 33rd AIAA Applied Aerodynamics Conference, Aviation 2015, Dallas, TX, June 22–26 2015.

[20] He, C. and Peters, D. A., "Comparison of Measured Induced Velocities with Results from a Closed-form Finite State Wake Model in Forward Flight", 45th Annual Forum of the American Helicopter Society International, Boston, MA, May 22-24, 1989.

[21] Govindarajan, B., and Leishman, J. G., "Prediction of Rotor and Rotor/Airframe Configurational Effects on Brownout Dust Clouds," *Journal of Aircraft* (Yet to appear, doi: 10.2514/1.C033447)

View publication stats